Auxiliary material for CERN-EP-2016-036

RA2/b Team

March 25, 2016

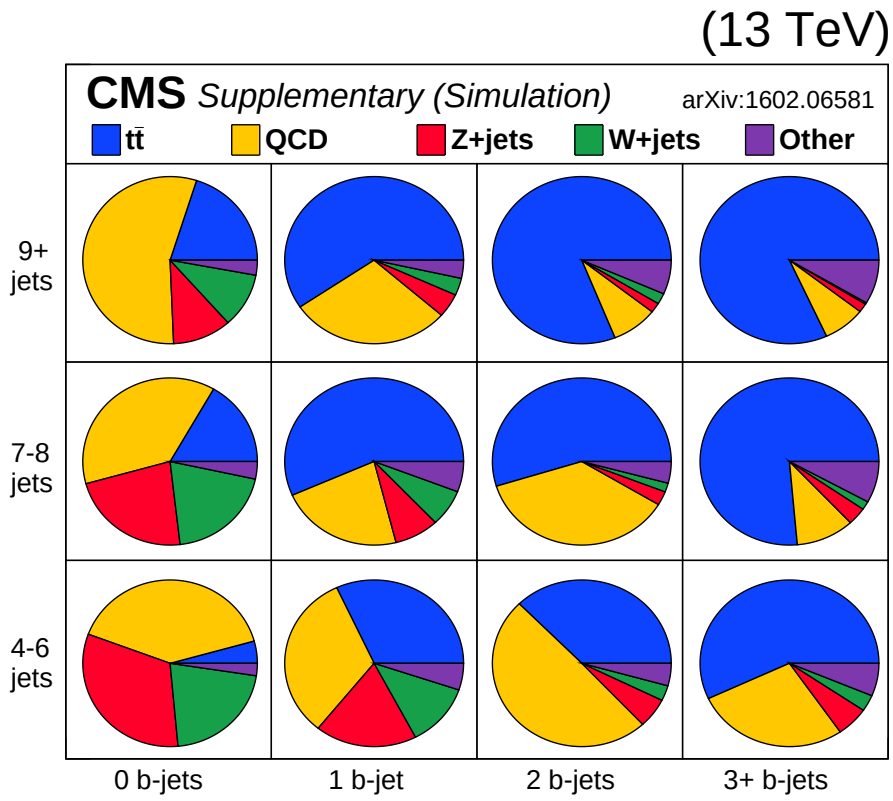

Figure 1: Background composition in zero-lepton search region ($H_{\mathrm{T}}^{\mathrm{miss}} > 200$ GeV, $H_{\mathrm{T}} > 500$ GeV) in bins of the number of jets and the number of b-tagged jets. The expected contribution from each process is obtained from simulation after applying the full baseline selection.

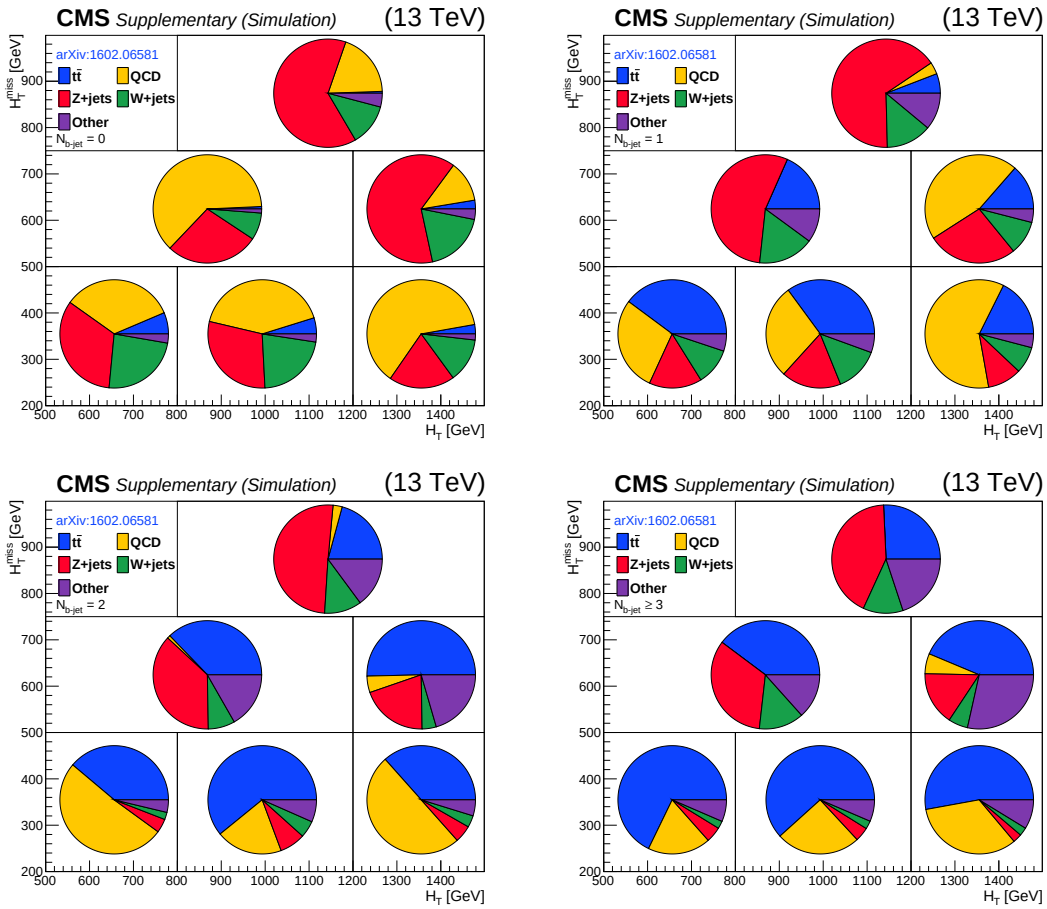

Figure 2: Background composition from simulation in zero-lepton search region in bins of $H_{\mathrm{T}}^{\mathrm{miss}}$ and H_{T}. The composition is shown separately for events with (top-left) 0 b-tagged jets, (top-right) 1 b-tagged jet, (bottom-left) 2 b-tagged jets, and (bottom-left) at least 3 b-tagged jets.

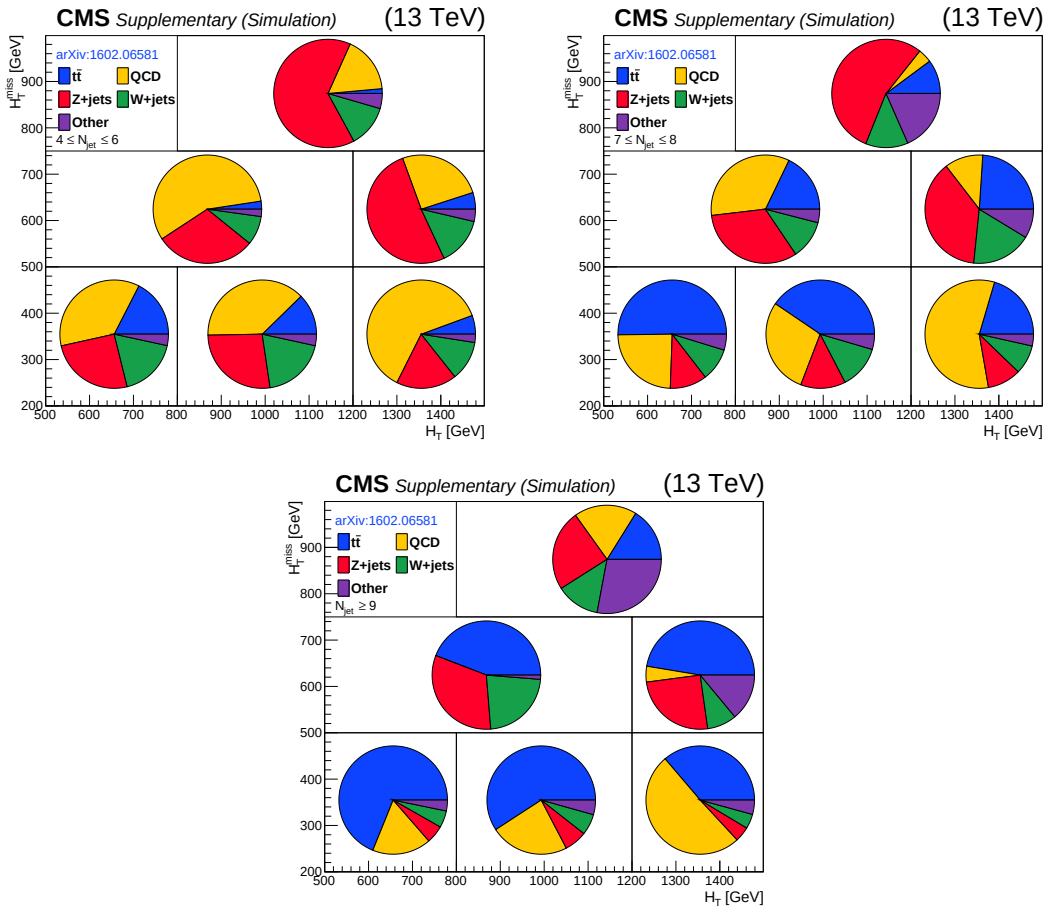

Figure 3: Background composition from simulation in zero-lepton search region in bins of $H_{\mathrm{T}}^{\mathrm{miss}}$ and H_{T}. The composition is shown separately for events with (left) 4-6 jets, (middle) 7-8 jets, and (right) at least 9 jets.

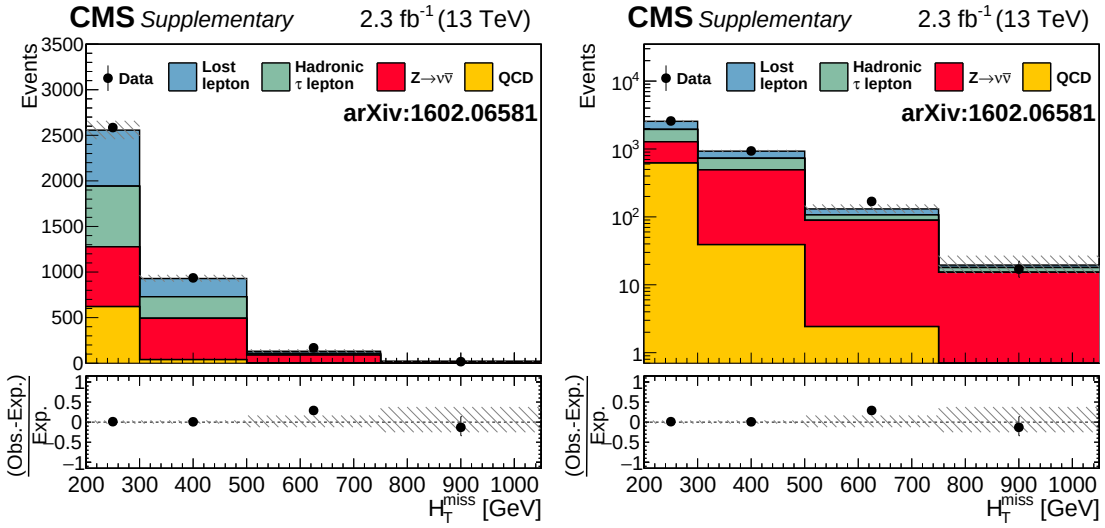

Figure 4: The distributions of observed number of events and predicted background as a function of $H_{\mathrm{T}}^{\mathrm{miss}}$, plotted on linear (left) and log (right) scales. Distributions are integrated over other binned observables in the analysis, number of b-tagged jets, number of jets, and H_{T}.

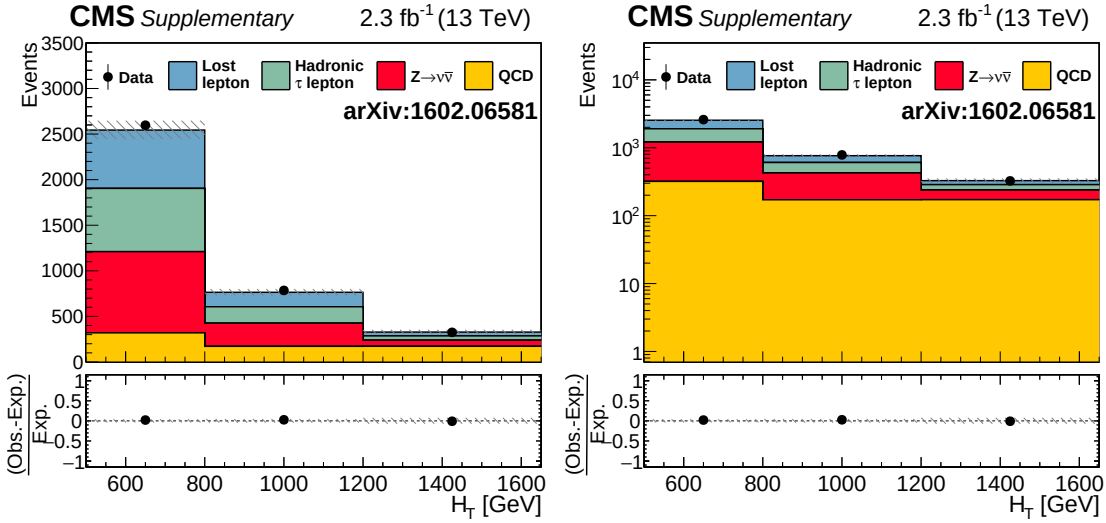

Figure 5: The distributions of observed number of events and predicted background as a function of H_{T}, plotted on linear (left) and log (right) scales. Distributions are integrated over other binned observables in the analysis, number of b-tagged jets, number of jets, and $H_{\mathrm{T}}^{\mathrm{miss}}$.

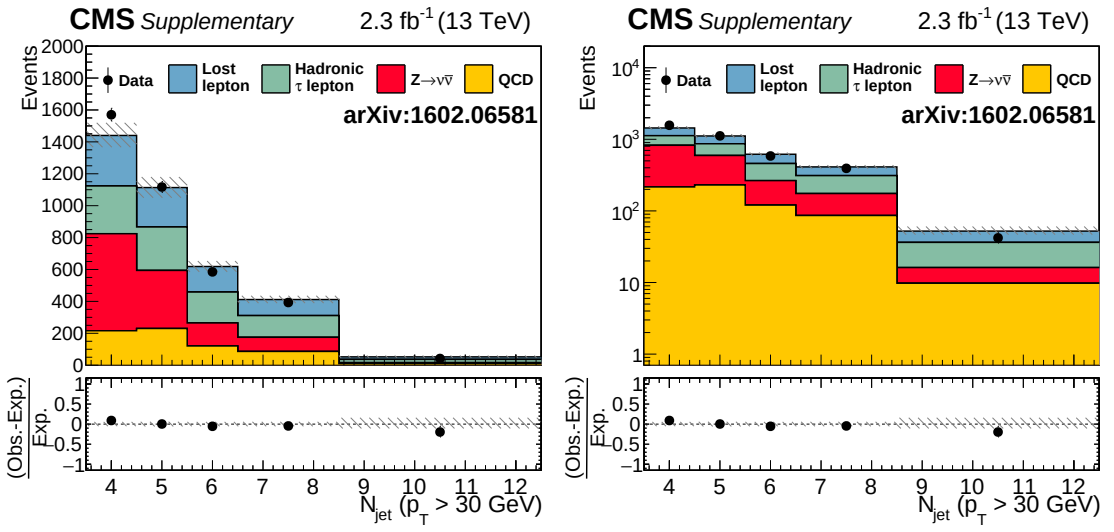

Figure 6: The distributions of observed number of events and predicted background as a function of the number of jets, plotted on linear (left) and log (right) scales. Distributions are integrated over other binned observables in the analysis, number of b-tagged jets, $H_{\mathrm{T}}^{\mathrm{miss}}$, and H_{T}.

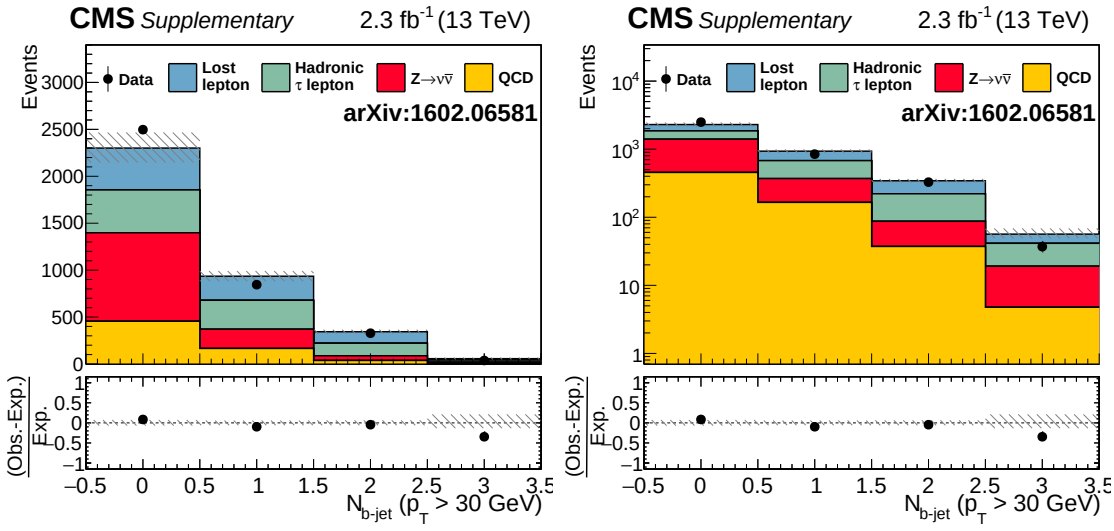

Figure 7: The distributions of observed number of events and predicted background as a function of the number of b-tagged jets, plotted on linear (left) and log (right) scales. Distributions are integrated over other binned observables in the analysis, number of jets, $H_{\mathrm{T}}^{\mathrm{miss}}$, and H_{T}.

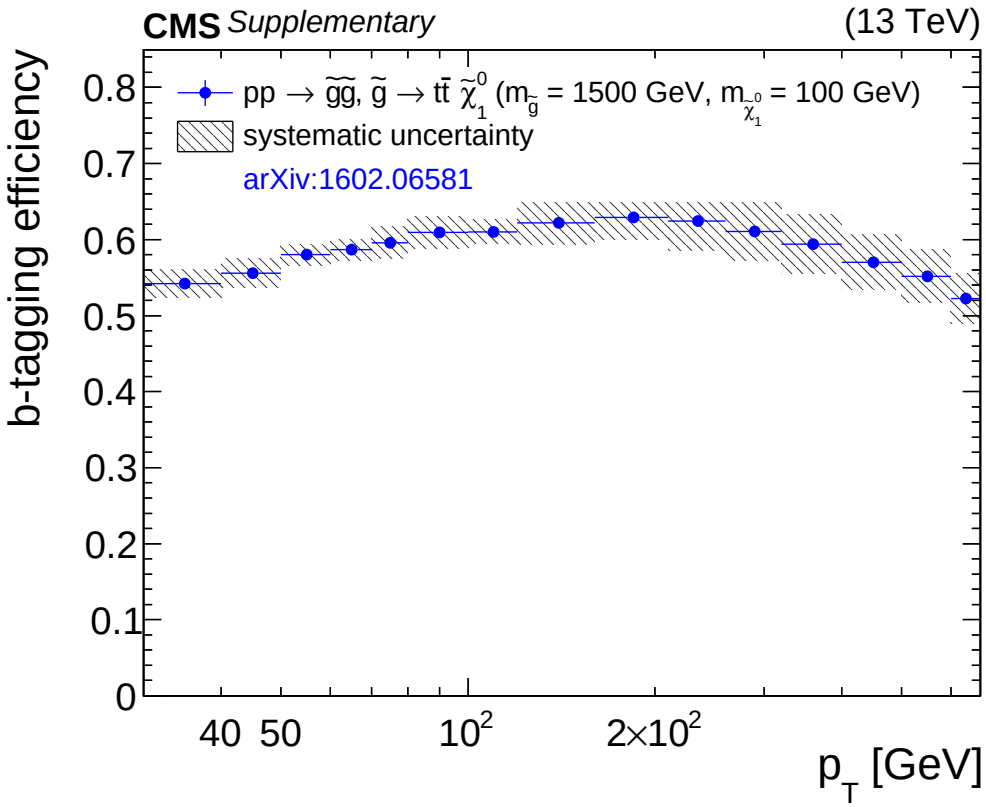

Figure 8: The b-tagging efficiency, with data/MC scale factors applied, for a representative signal model. Statistical and systematic uncertainties are shown separately.

$\mathrm{pp} \to \widetilde{\mathrm{g}}\widetilde{\mathrm{g}}, \widetilde{\mathrm{g}} \to \mathrm{t}\bar{\mathrm{t}}\widetilde{\chi}_1^0$ ($m_{\widetilde{\mathrm{g}}} = 1500\,\mathrm{GeV}, m_{\widetilde{\chi}_1^0} = 100\,\mathrm{GeV}$)

p_T [GeV]		$\varepsilon_{\text{b-tagging}} \pm$ stat. unc. $\pm$ syst. unc.		
30	40	0.542 $\pm$	0.004 $\pm$	0.019
40	50	0.556 $\pm$	0.004 $\pm$	0.019
50	60	0.580 $\pm$	0.004 $\pm$	0.013
60	70	0.587 $\pm$	0.004 $\pm$	0.014
70	80	0.596 $\pm$	0.004 $\pm$	0.021
80	100	0.610 $\pm$	0.003 $\pm$	0.021
100	120	0.610 $\pm$	0.003 $\pm$	0.016
120	160	0.622 $\pm$	0.002 $\pm$	0.029
160	210	0.629 $\pm$	0.002 $\pm$	0.029
210	260	0.625 $\pm$	0.003 $\pm$	0.039
260	320	0.610 $\pm$	0.003 $\pm$	0.038
320	400	0.594 $\pm$	0.003 $\pm$	0.039
400	500	0.570 $\pm$	0.004 $\pm$	0.037
500	600	0.552 $\pm$	0.004 $\pm$	0.035
600	670	0.523 $\pm$	0.006 $\pm$	0.033

Figure 9: The b-tagging efficiency in table form, with data/MC scale factors applied, for a representative signal model. Statistical and systematic uncertainties are shown separately.

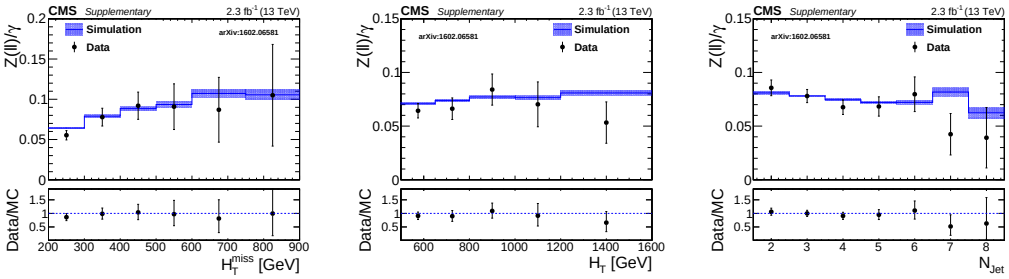

Figure 10: The $Z \to \ell^+\ell^-/\gamma$ ratio as a function of $H_{\mathrm{T}}^{\mathrm{miss}}$ (left), H_{T} (middle), and the number of jets (right) after baseline selection. The $Z \to \nu\bar{\nu}/\gamma$ transfer factor is computed using simulated events and we check in one dimensional projections that data agree with simulation.

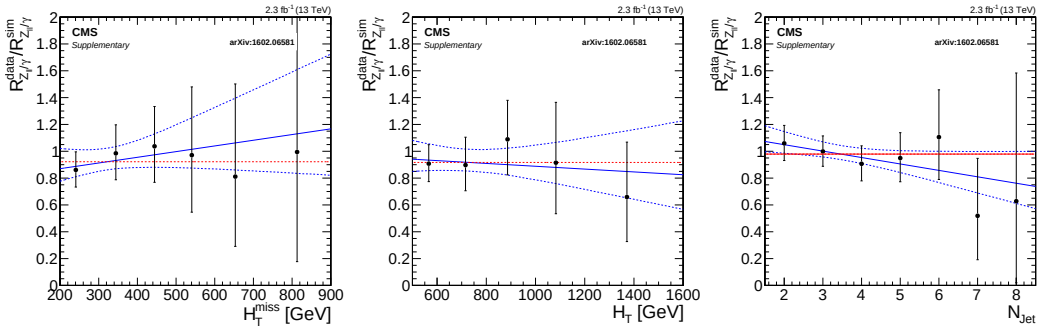

Figure 11: The $Z \to \ell^+\ell^-/\gamma$ Double Ratio and linear fit as a function of $H_{\mathrm{T}}^{\mathrm{miss}}$ (left), H_{T} (middle), and the number of jets (right) after baseline selection. The average value of 0.924 is drawn as a red dashed line.

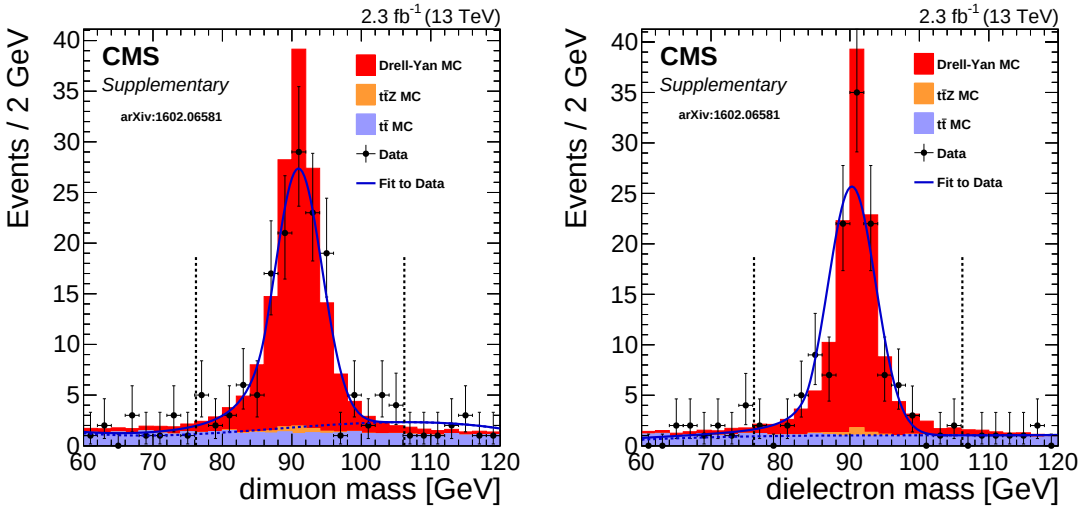

Figure 12: The dimuon (left) and dielectron (right) invariant mass distributions of the $Z \to \ell^+\ell^-$ control regions. Fit shapes are obtained from a data sample with baseline selection, except for a loosening of the selection on the number of jets to 2. These shapes are then fixed and fit to the baseline selection as shown.

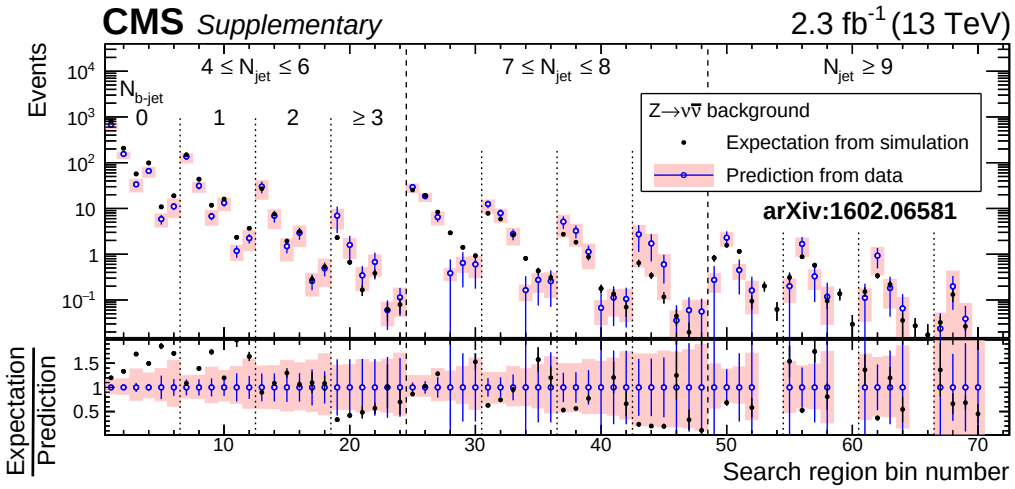

Figure 13: Predicted $(Z \to \nu\bar{\nu}) +$ jets yields in the full 72-bin search space, from $\gamma +$ jets data (for 0 b-tagged jets) combined with the extrapolation factors from $(Z \to \ell^+\ell^-) +$ jets (for at least 1 b-tagged jet). Statistical (blue error bars) and systematic (pink shaded) uncertainties are plotted separately, and for comparison the expectation from simulation is overlaid as the black points with (statistical) error bars.

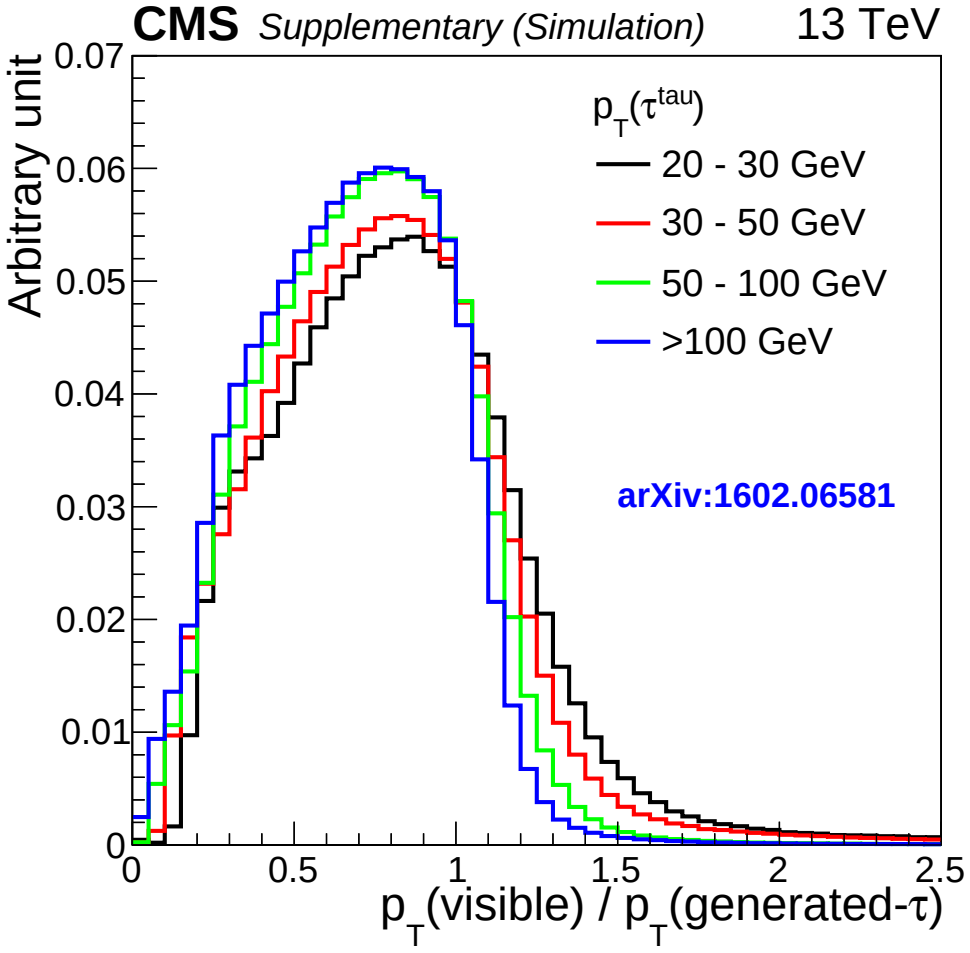

Figure 14: The τ_h response templates: the distribution of $\frac{p_{\mathrm{T},\,\tau_{\mathrm{h-reco}}}}{p_{\mathrm{T},\,\tau_{\mathrm{h-gen}}}}$ in intervals of $p_{\mathrm{T},\,\tau_{\mathrm{h-gen}}}$, as determined from simulated $\mathrm{t\bar{t}}$ and W+jets events.

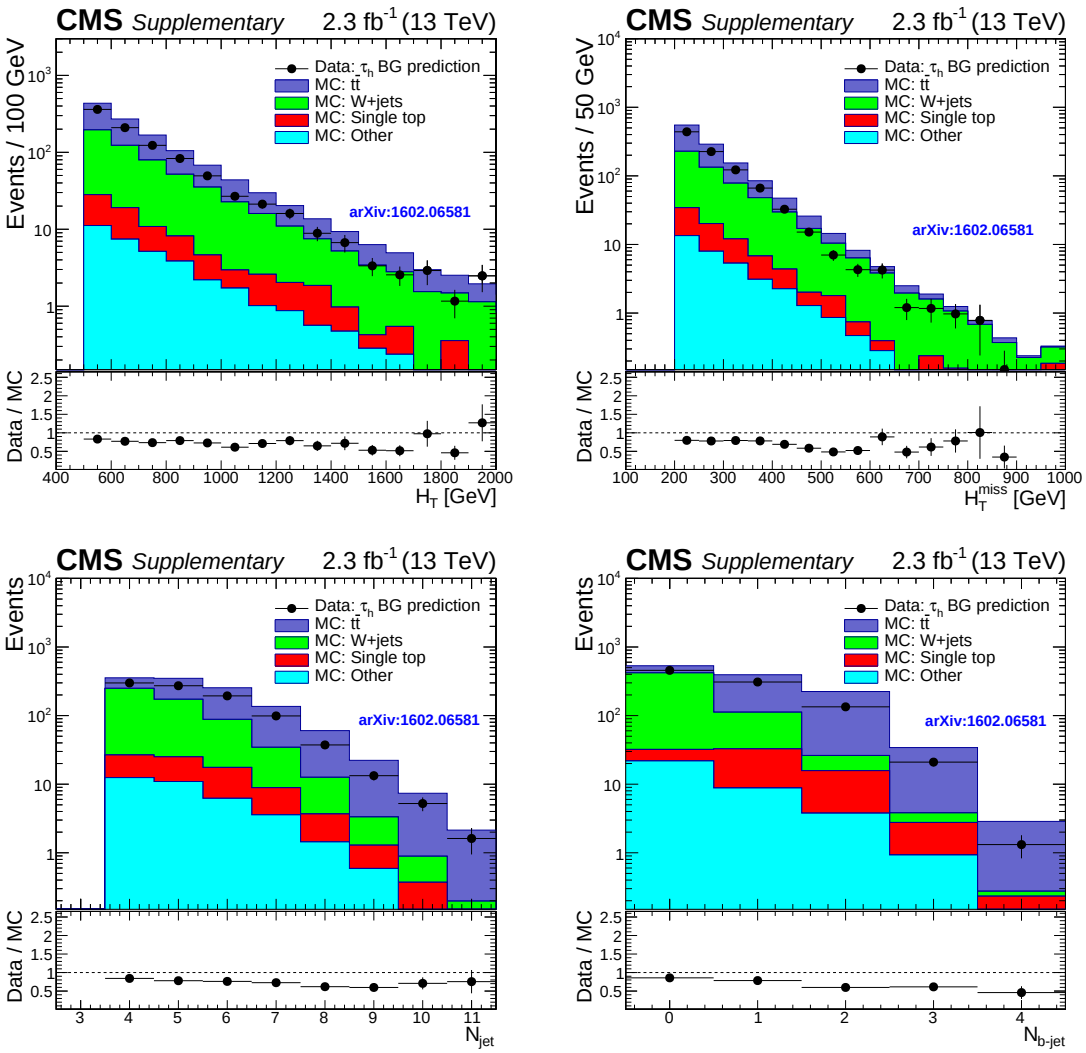

Figure 15: Clockwise from top-left, distributions of H_{T}, $H_{\mathrm{T}}^{\mathrm{miss}}$, the number of b-tagged jets, and the number of jets in τ_h background events as predicted by performing the data driven background-determination procedure on the 2.3 fb^{-1} of data (shaded regions), compared to the τ_h background expectation from simulation (solid points) for the baseline selection. The simulation includes $\mathrm{t\bar{t}}$, W+jets, single top quark, and other rare SM process events.

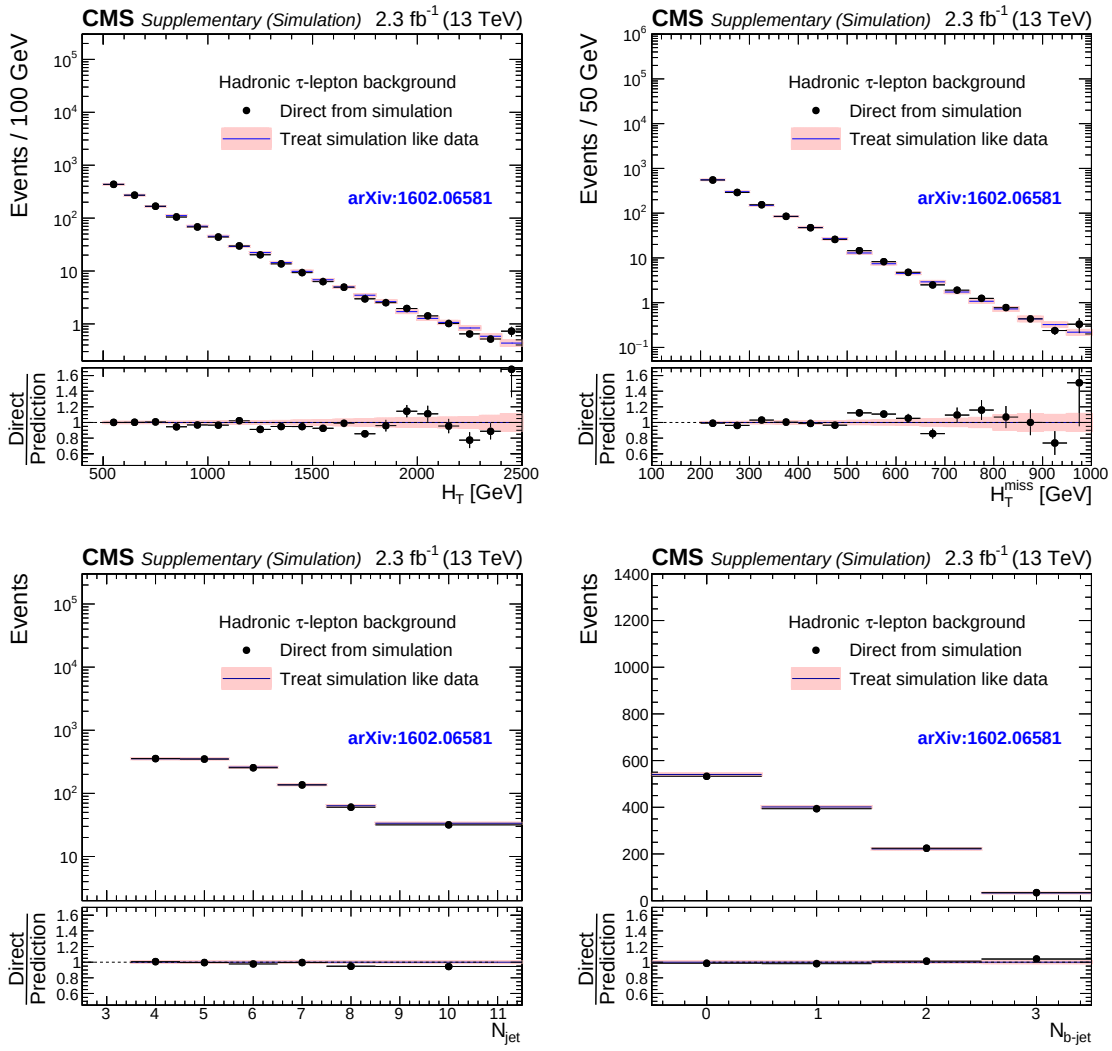

Figure 16: Clockwise from top-left, distributions of H_{T}, $H_{\mathrm{T}}^{\mathrm{miss}}$, the number of b-tagged jets, and the number of jets in τ_h background events as predicted directly from simulation (solid points) and as predicted by the data-driven background-determination procedure (shaded regions), for the baseline selection. The simulation simulation includes $\mathrm{t\bar{t}}$, W+jets, single-top, Drell-Yan, and other rare SM process events.

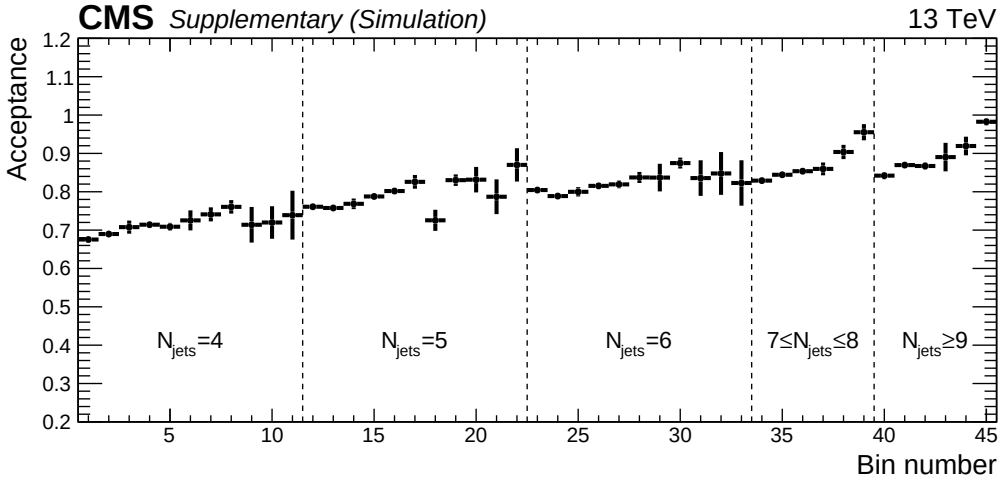

Figure 17: Acceptance ϵ^{μ}_{Acc} of hadronically-decaying τ leptons for $p_T > 20$ GeV and $\eta < 2.1$. The results are shown as a function of $H_{\mathrm{T}}^{\mathrm{miss}}$, H_{T}, and N_{jet}, integrated over the four bins of $N_{\mathrm{b-jet}}$ (in total 45 bins).

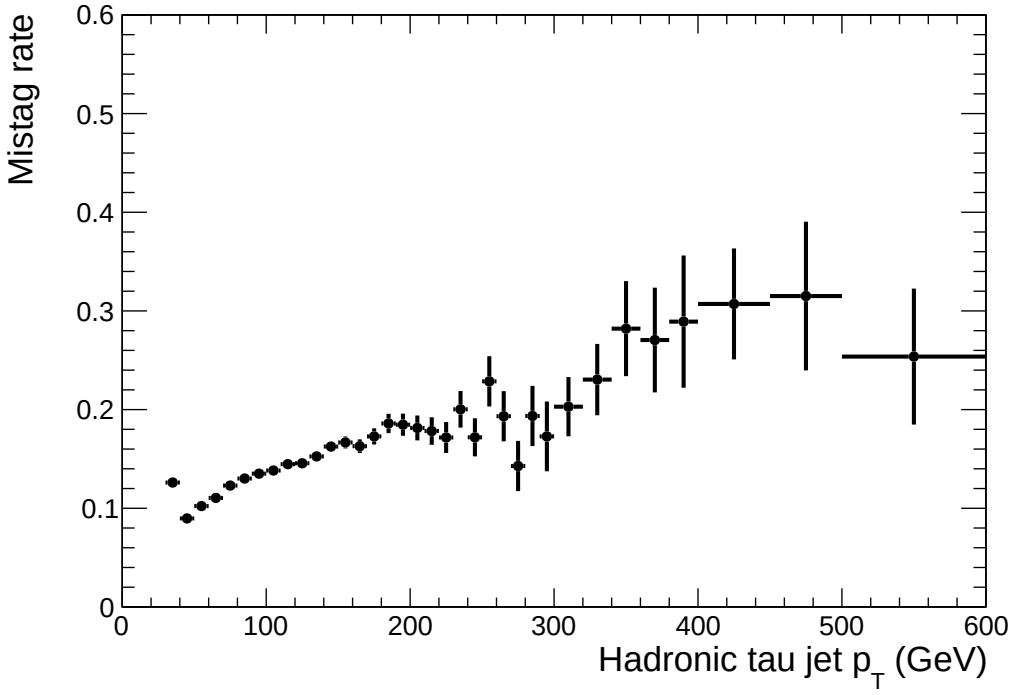

Figure 18: The mistag rate of τ_h jet as function of transverse momentum.

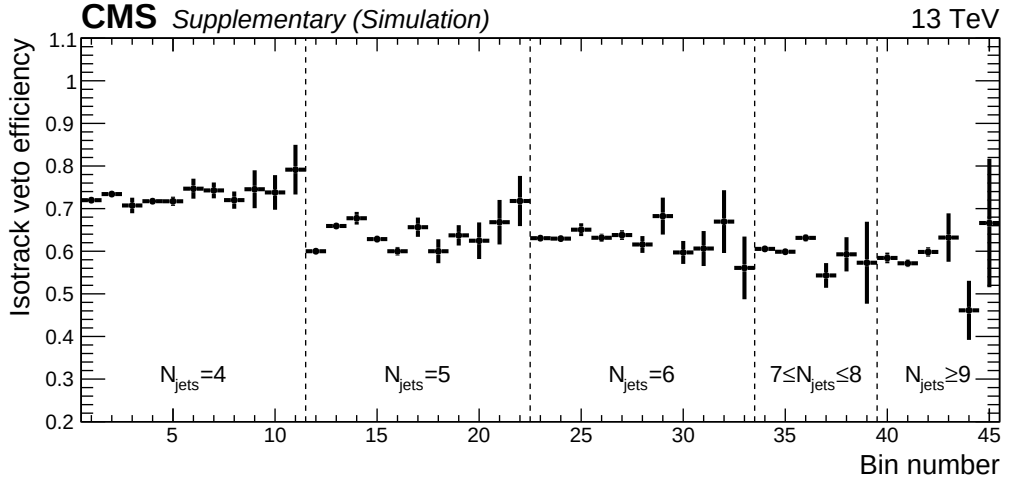

Figure 19: The isolated-track veto efficiency ϵ_{isotrk}. The results are shown as a function of $H_{\mathrm{T}}^{\mathrm{miss}}$, H_{T}, and N_{jet}, integrated over the four bins of $N_{\mathrm{b-jet}}$ (in total 45 bins).

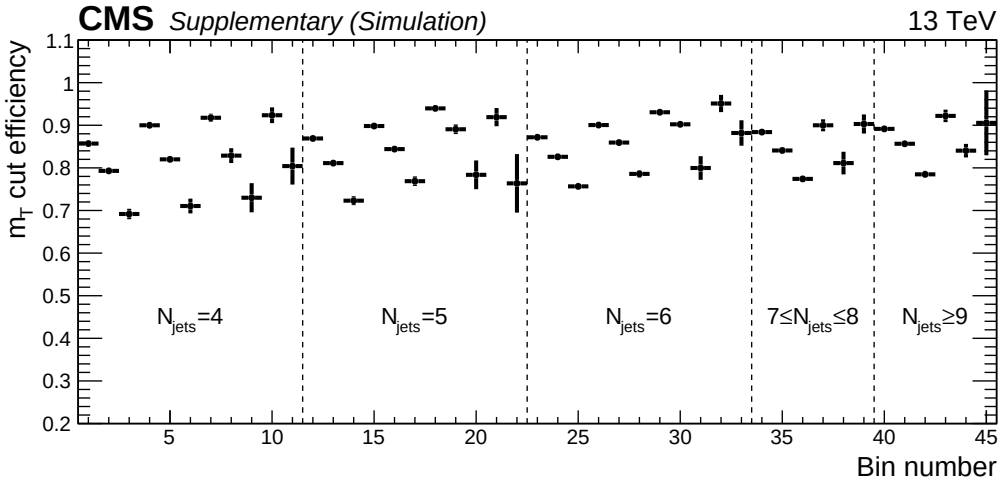

Figure 20: The efficiency ϵ_{m_T} of the muon m_T selection. The results are shown as a function of $H_{\mathrm{T}}^{\mathrm{miss}}$, H_{T}, and N_{jet}, integrated over the four bins of $N_{\mathrm{b-jet}}$ (in total 45 bins).

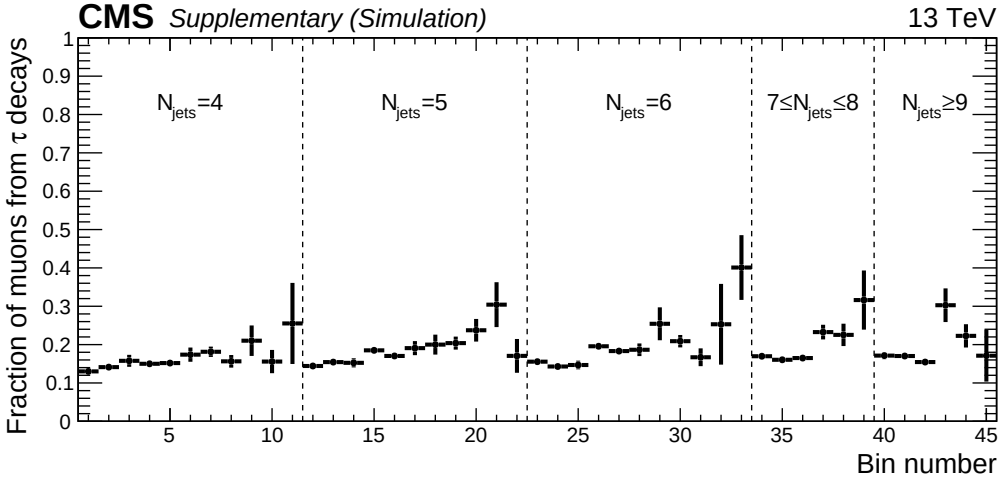

Figure 21: The fraction f of muons from τ decays in the single-muon control sample, as determined from simulation. The results are shown as a function of $H_{\mathrm{T}}^{\mathrm{miss}}$, H_{T}, and N_{jet}, integrated over the four bins of $N_{\mathrm{b-jet}}$ (in total 45 bins).

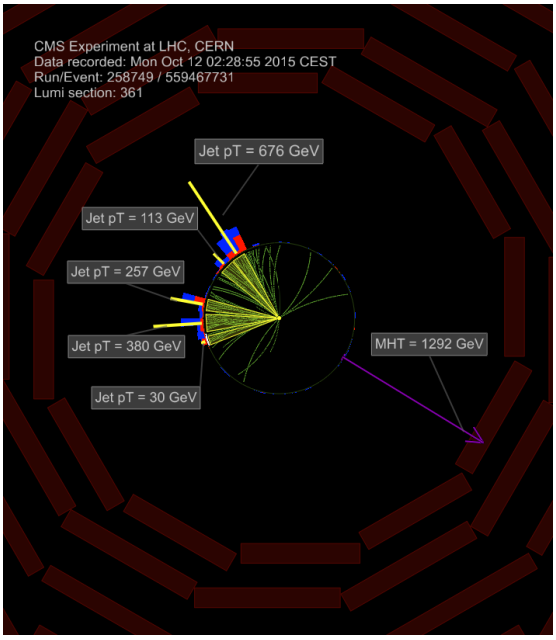

Figure 22: Event display showing the $\rho - \phi$ plane for event 258749:361:559467731, which has the highest observed $H_{\mathrm{T}}^{\mathrm{miss}}$ of all events in the search region. Only tracks with $p_T > 1.5$ GeV are shown.

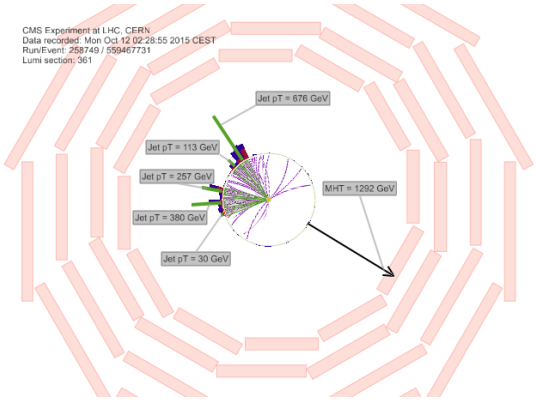

Figure 23: Event display showing the $\rho - \phi$ plane for event 258749:361:559467731, with a white background.

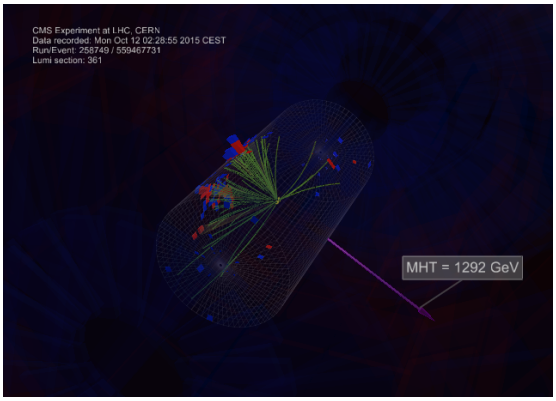

Figure 24: Event display showing the $\rho - \phi$ plane for event 258749:361:559467731, showing the event in 3D Tower view mode..

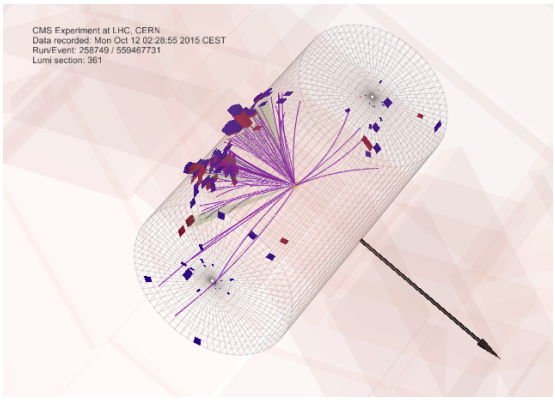

Figure 25: Event display showing the $\rho - \phi$ plane for event 258749:361:559467731, showing the event in 3D Tower view mode with a white background.

Selection	$pp \to \widetilde{g}\widetilde{g}, \widetilde{g} \to b\bar{b}\widetilde{\chi}_1^0$ $m_{\widetilde{g}} = 1500\,\text{GeV}$ $m_{\widetilde{\chi}_1^0} = 100\,\text{GeV}$	$pp \to \widetilde{g}\widetilde{g}, \widetilde{g} \to t\bar{t}\widetilde{\chi}_1^0$ $m_{\widetilde{g}} = 1500\,\text{GeV}$ $m_{\widetilde{\chi}_1^0} = 100\,\text{GeV}$	$pp \to \widetilde{g}\widetilde{g}, \widetilde{g} \to q\bar{q}\widetilde{\chi}_1^0$ $m_{\widetilde{g}} = 1000\,\text{GeV}$ $m_{\widetilde{\chi}_1^0} = 800\,\text{GeV}$
$N_{\text{jet}} \geq 4$	96.49 ± 0.08	99.96 ± 0.01	76.87 ± 0.14
$H_{\text{T}} > 500\,\text{GeV}$	96.46 ± 0.08	99.89 ± 0.01	38.30 ± 0.16
$H_{\text{T}}^{\text{miss}} > 200\,\text{GeV}$	87.21 ± 0.15	88.65 ± 0.10	24.46 ± 0.14
$N_{\text{muon}} = 0$	86.59 ± 0.15	56.00 ± 0.15	24.42 ± 0.14
$N_{\text{isolated tracks}}^{(\text{muon})} = 0$	86.29 ± 0.15	54.87 ± 0.15	24.36 ± 0.14
$N_{\text{electron}} = 0$	85.66 ± 0.15	34.46 ± 0.15	24.19 ± 0.14
$N_{\text{isolated tracks}}^{(\text{electron})} = 0$	85.17 ± 0.16	33.50 ± 0.15	24.00 ± 0.14
$N_{\text{isolated tracks}}^{(\text{hadron})} = 0$	84.20 ± 0.16	31.57 ± 0.14	23.26 ± 0.14
$\Delta\phi_{H_{\text{T}}^{\text{miss}},j_1} > 0.5$	81.96 ± 0.17	30.68 ± 0.14	23.10 ± 0.14
$\Delta\phi_{H_{\text{T}}^{\text{miss}},j_2} > 0.5$	73.62 ± 0.19	27.39 ± 0.14	20.65 ± 0.13
$\Delta\phi_{H_{\text{T}}^{\text{miss}},j_3} > 0.3$	67.84 ± 0.20	25.58 ± 0.14	19.10 ± 0.13
$\Delta\phi_{H_{\text{T}}^{\text{miss}},j_4} > 0.3$	62.00 ± 0.21	23.96 ± 0.13	17.66 ± 0.12

Figure 26: An expanded and reorganized version of the table of absolute cumulative efficiencies in % for each step of the event selection process, listed for three representative signal models and choices for the gluino and LSP masses. The lepton and isolated track vetoes are grouped by lepton flavor (muon or electron) and each $\Delta\phi$ cut is shown separately. Only statistical uncertainties are shown.

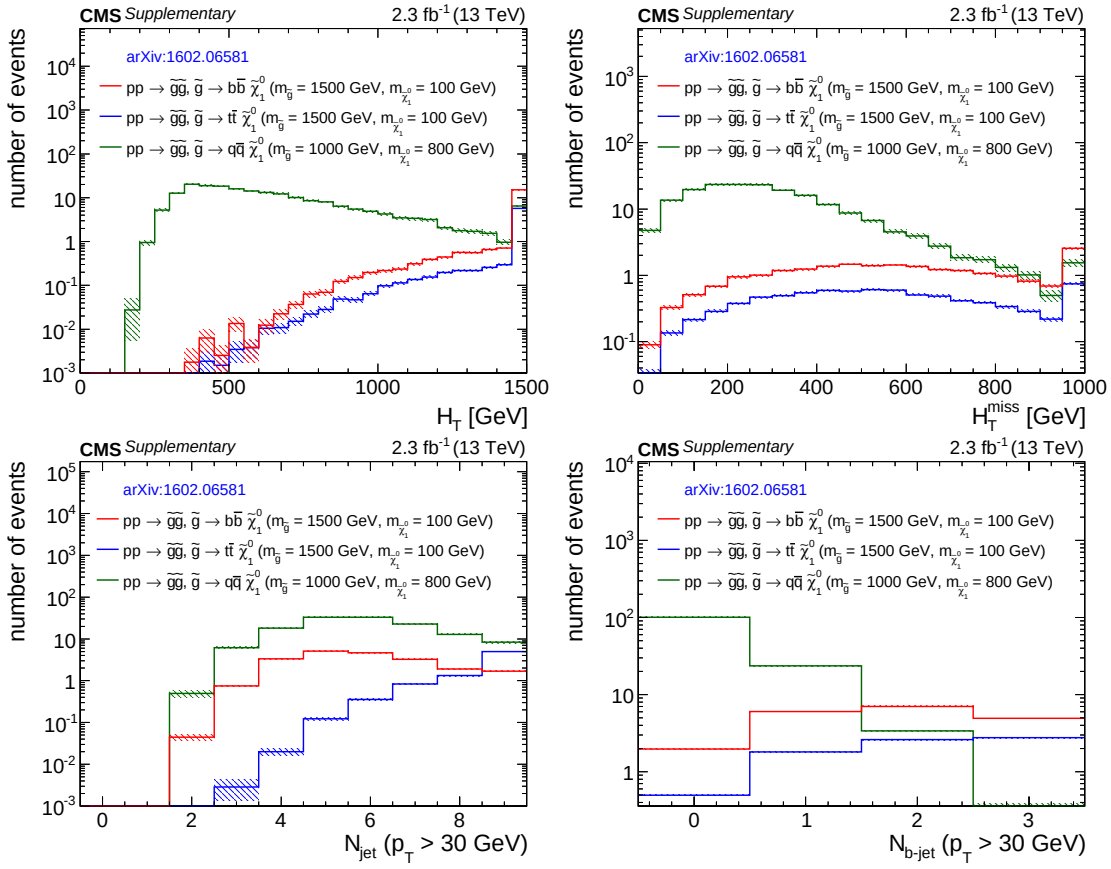

Figure 27: Clockwise from top-left, distributions of H_{T}, $H_{\mathrm{T}}^{\mathrm{miss}}$, the number of b-tagged jets, and the number of jets from three representative signal models after the baseline selection. Each plot ignores the baseline requirement (if any) for its respective variable. The last bin in each plot contains the overflow events. Only statistical uncertainties are shown.

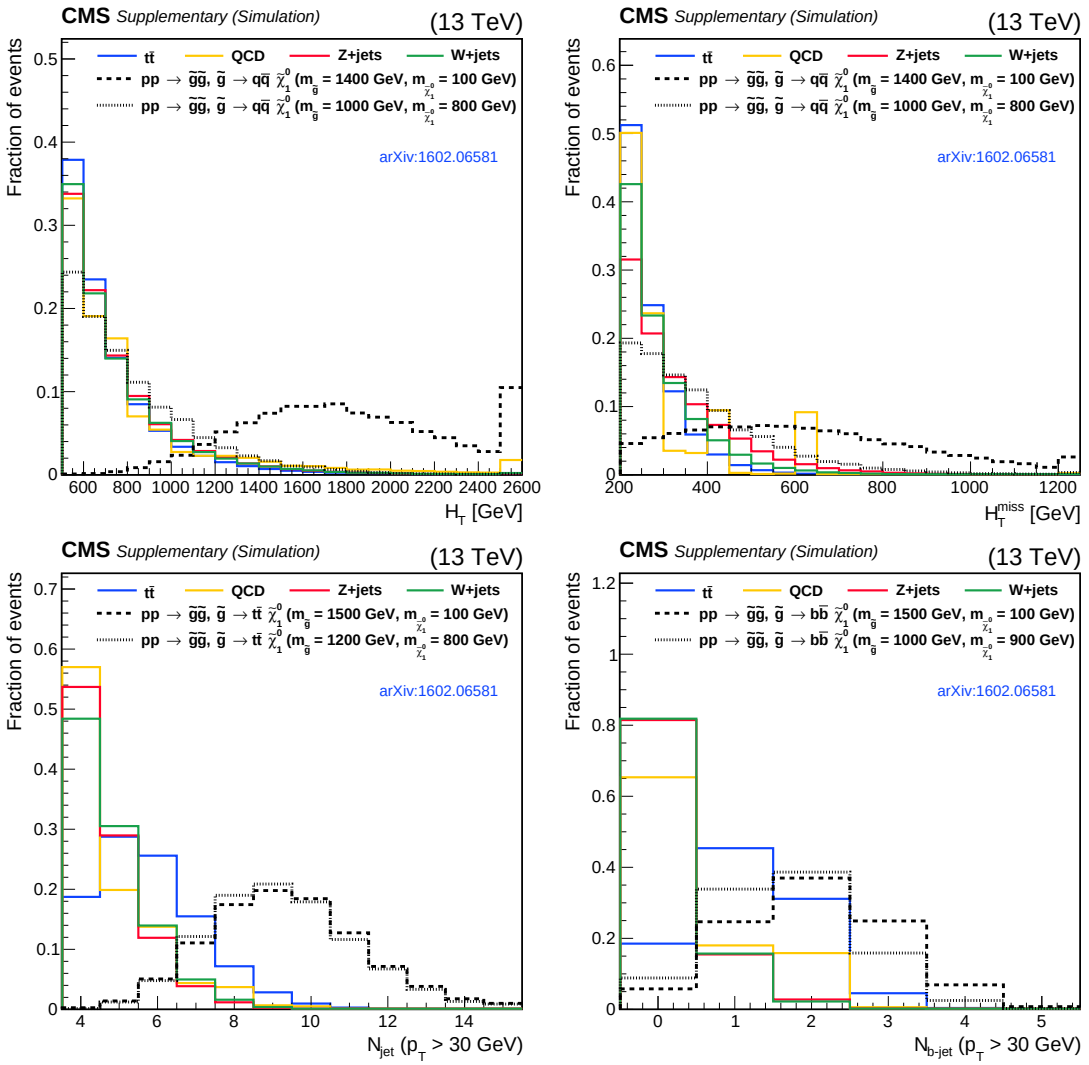

Figure 28: Clockwise from top-left, kinematic shape comparisons showing distributions of H_{T}, $H_{\mathrm{T}}^{\mathrm{miss}}$, the number of b-tagged jets, and the number of jets for the main background processes and six example gluino production signal models. The full baseline selection is applied in each plot.

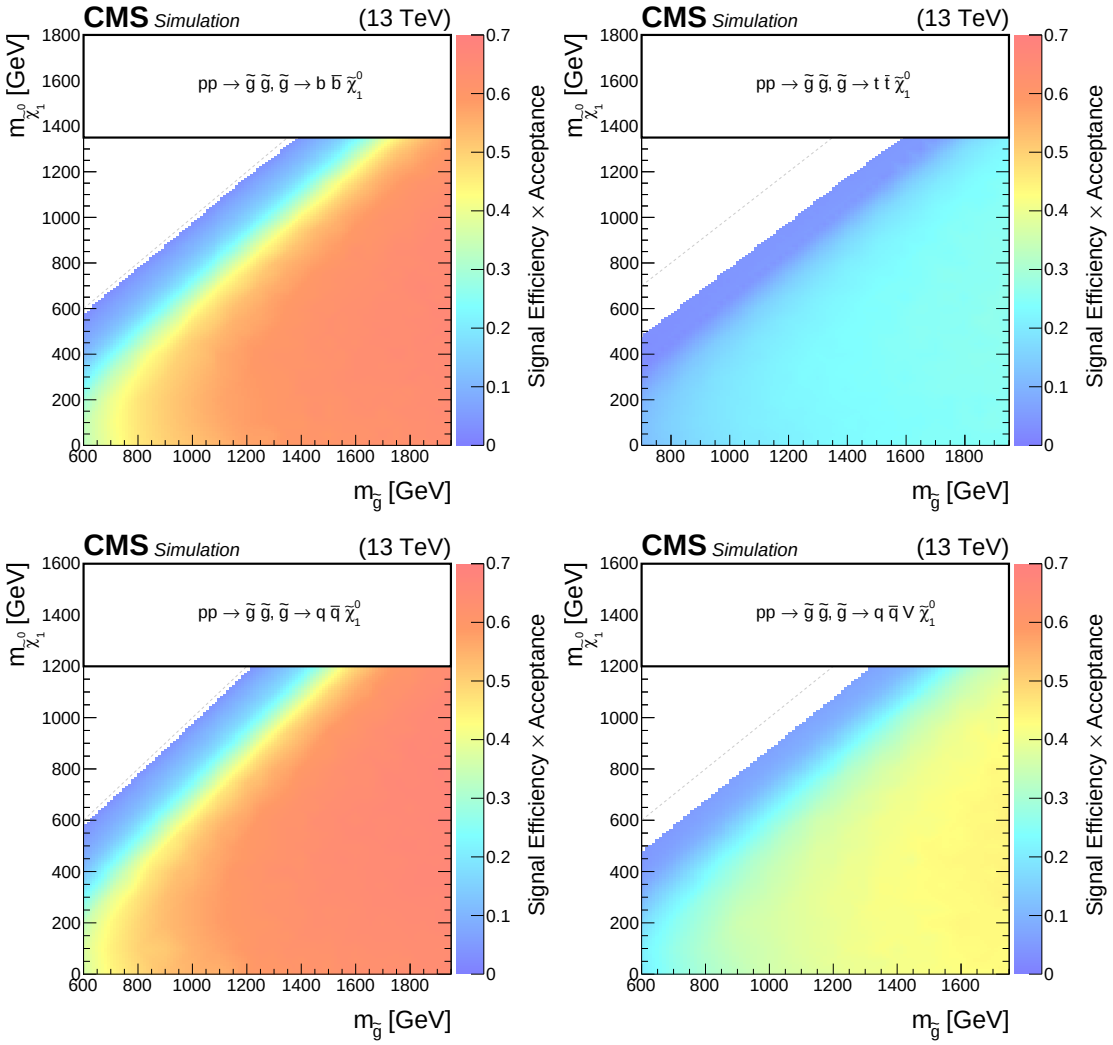

Figure 29: The product of signal efficiency and acceptance for the baseline selection in the $m_{\tilde{\chi}_1^0} - m_{\tilde{g}}$ mass plane. Clockwise from top-left are the SMS models T1bbbb, T1tttt, T5qqqqVV, T1qqqq.

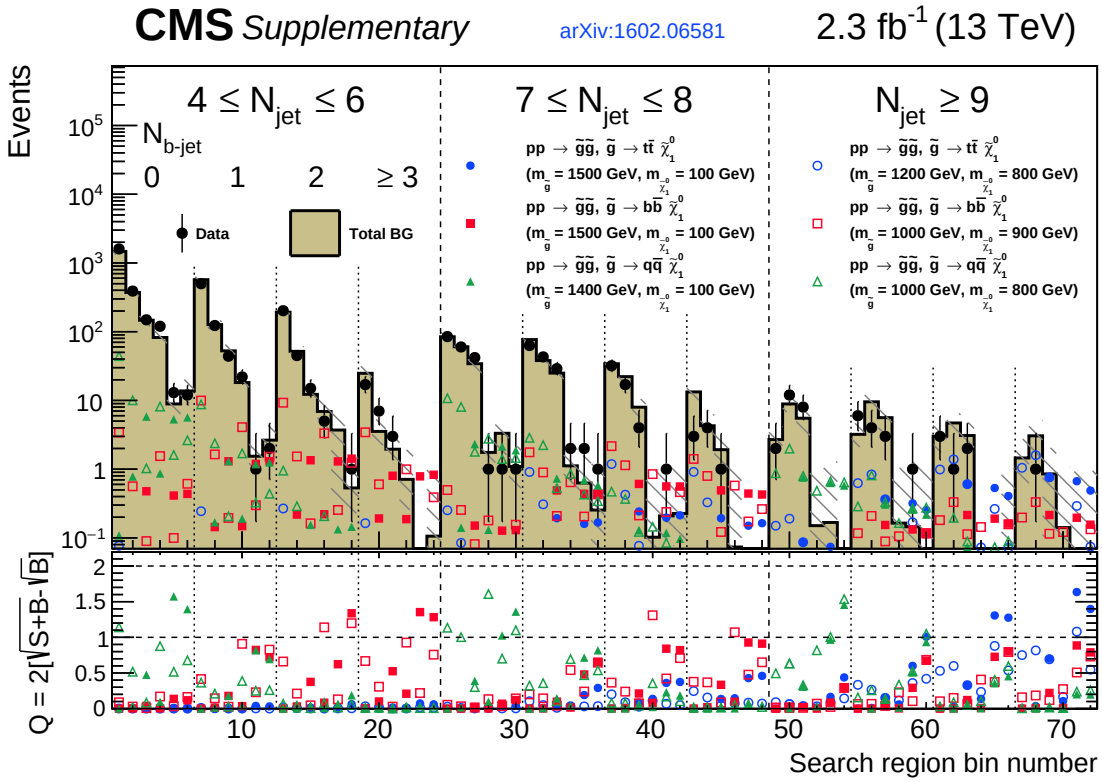

Figure 30: The sensitivity of the analysis to different direct gluino production signal models as a function of the analysis binning. The upper panel shows the total predicted SM backgrounds and the expected number of signal events for six representative model points per analysis bin. The bottom panel shows the expected sensitivity, expressed in terms of the figure of merit Q, per analysis bin.

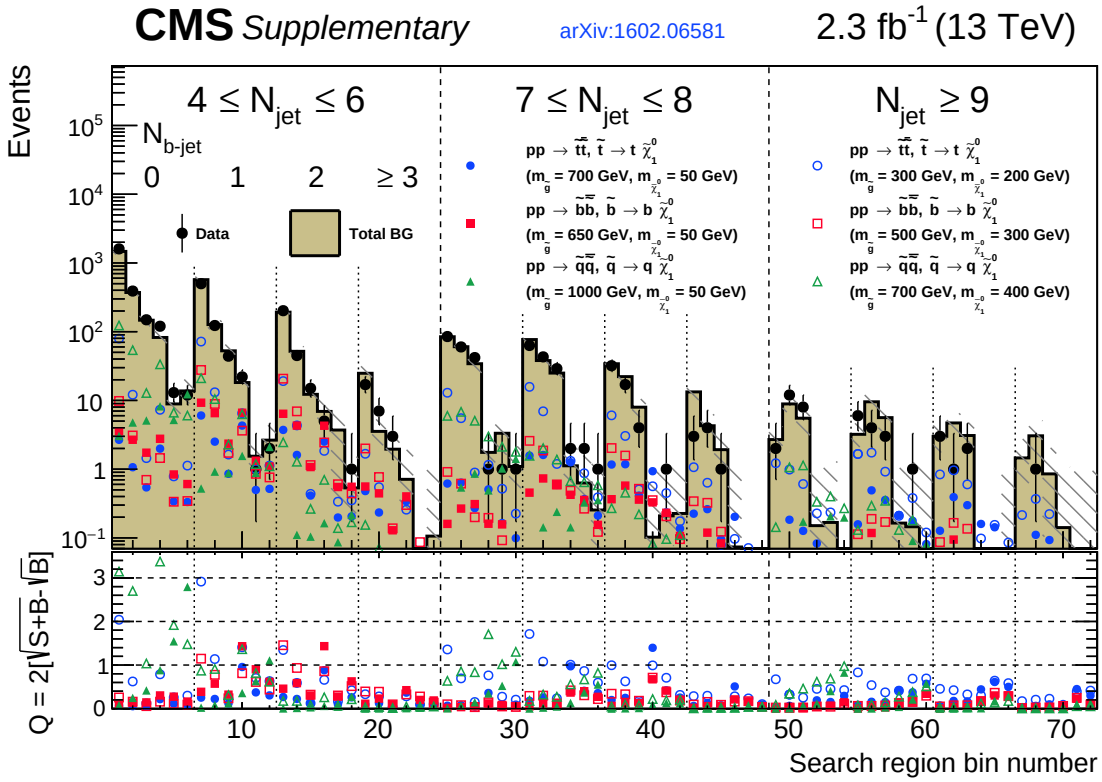

Figure 31: The sensitivity of the analysis to different direct squark production signal models as a function of the analysis binning. The upper panel shows the total predicted SM backgrounds and the expected number of signal events for six representative model points per analysis bin. The bottom panel shows the expected sensitivity, expressed in terms of the figure of merit Q, per analysis bin.

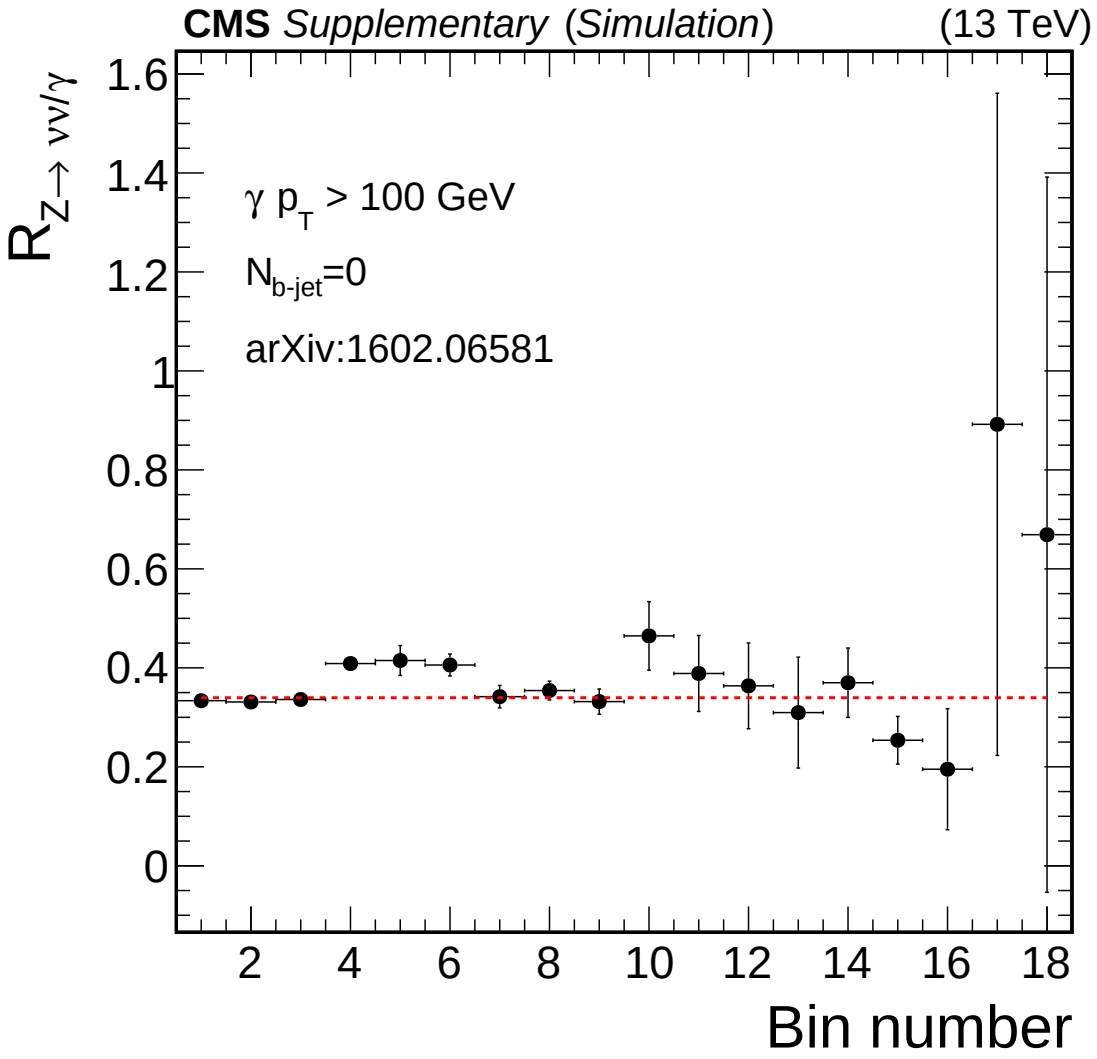

Figure 32: The Z($\nu\nu$)/γ ratio calculated using leading order Monte Carlo simulation in the search bins with $N_{\mathrm{b-jet}} = 0$.

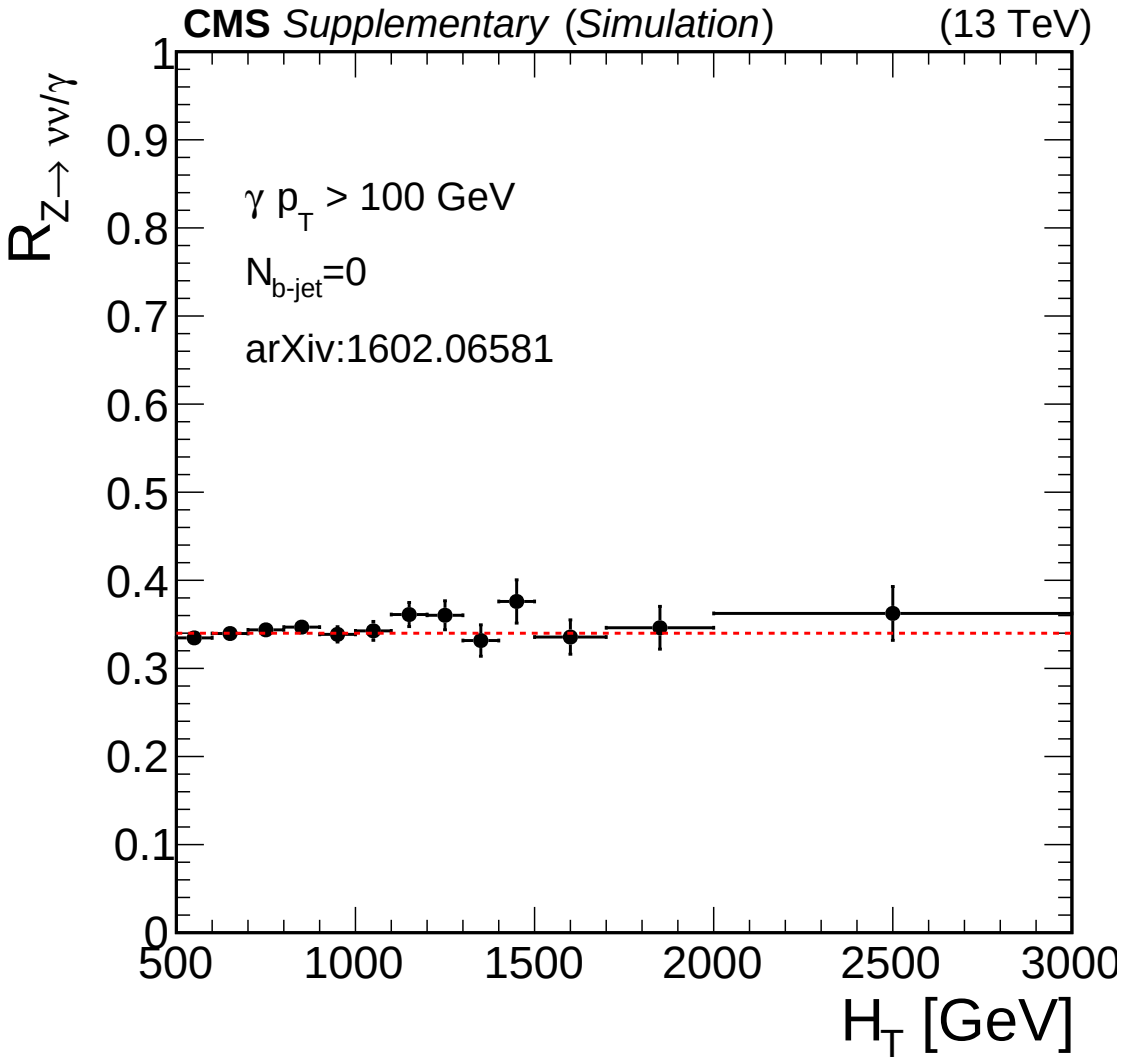

Figure 33: The Z($\nu\nu$)/γ ratio vs. H_{T} calculated using leading order Monte Carlo simulation.

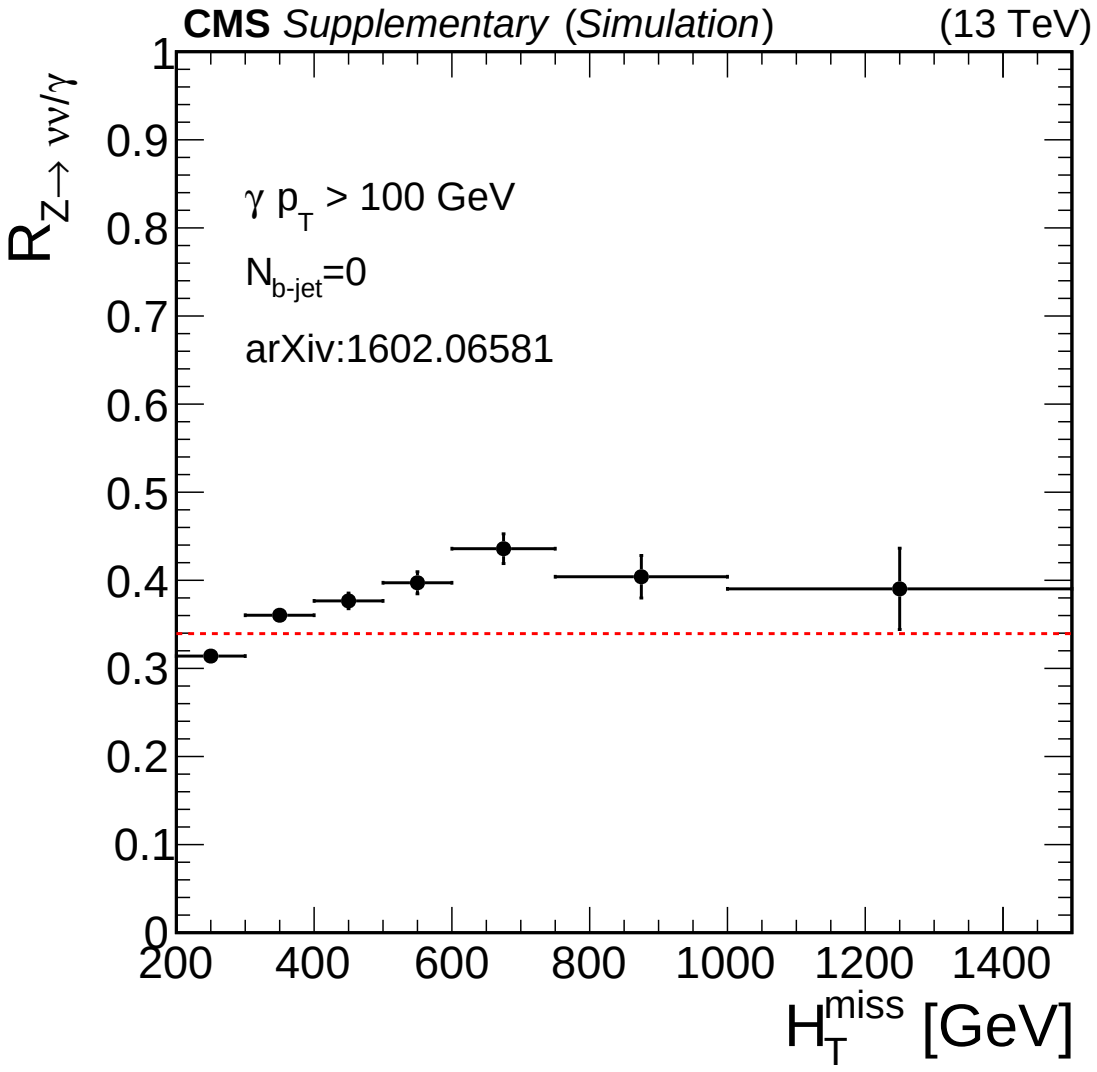

Figure 34: The Z($\nu\nu$)/γ ratio vs. $H_{\mathrm{T}}^{\mathrm{miss}}$ calculated using leading order Monte Carlo simulation.

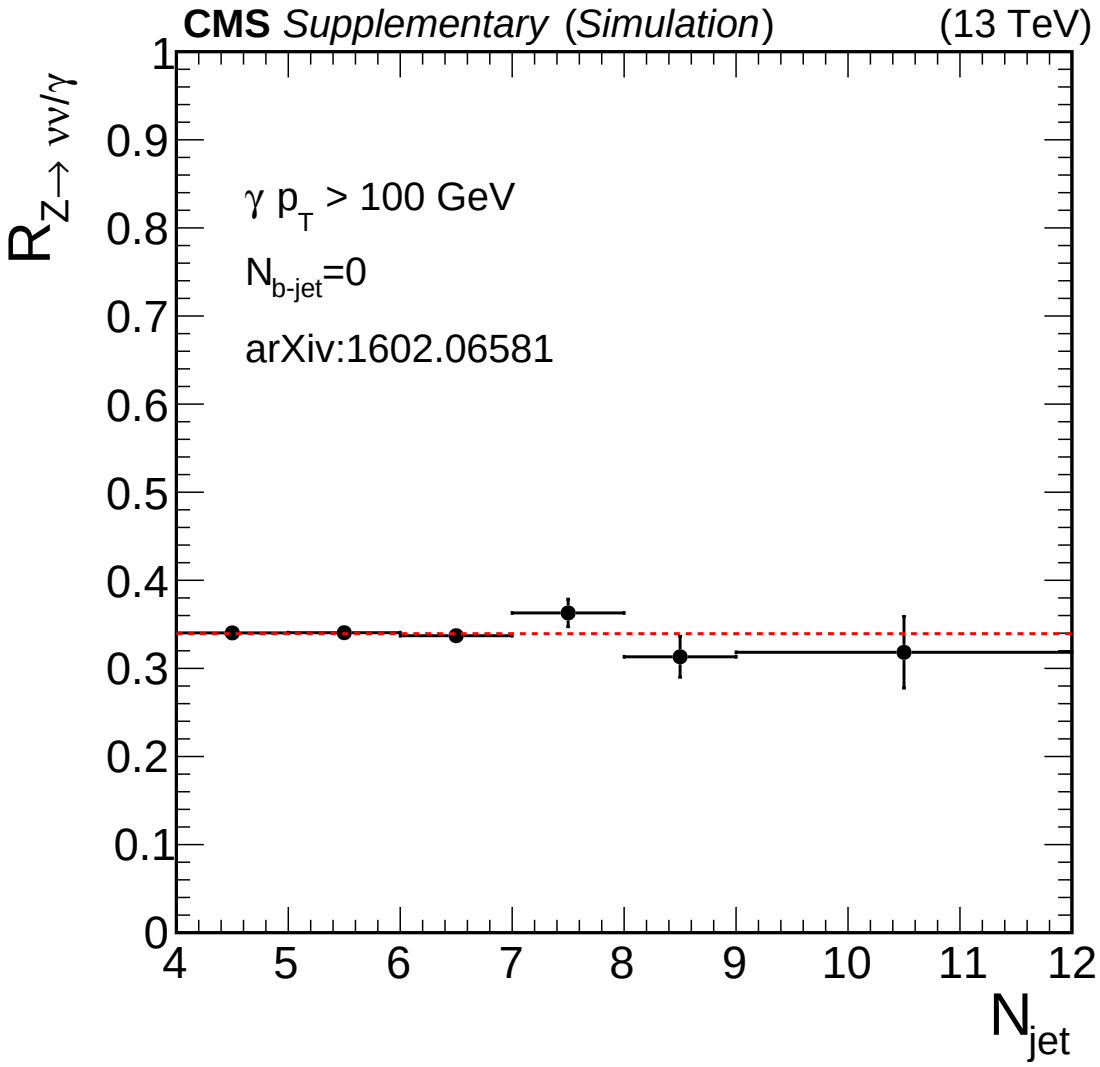

Figure 35: The Z($\nu\nu$)/γ ratio vs. N_{jet} calculated using leading order Monte Carlo simulation.

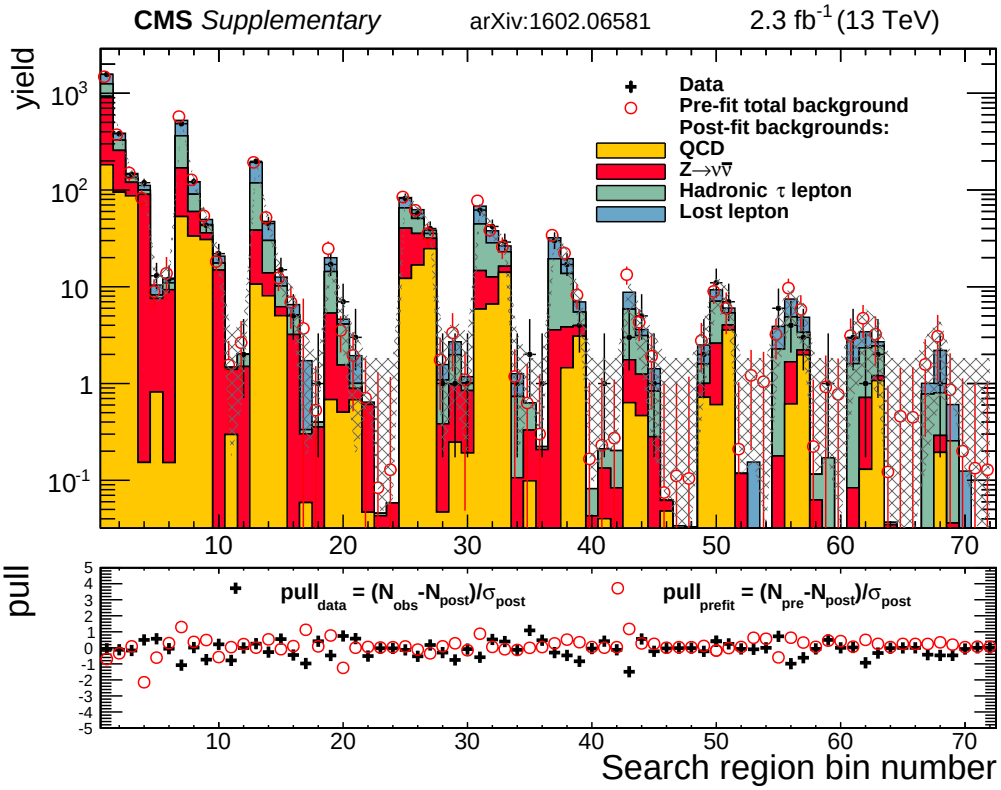

Figure 36: Observed numbers of events and corresponding SM background predictions in the 72 search regions of the analysis after the final fit performed with the assumption of only standard model contributions. Background predictions before the final fit are also shown for comparison. The lower panel shows the pull distributions for the data and the pre-fit background estimates with respect to the post-fit background estimates.

Table 1: Expected numbers of events in search bins with $4 \leq N_{\text{jet}} \leq 6$ for three representative signal models. Only statistical uncertainties are shown.

Bin	$H_{\text{T}}^{\text{miss}}$ [GeV]	H_{T} [GeV]	$N_{\text{b-jet}}$	$pp \to \tilde{\text{g}}\tilde{\text{g}}, \tilde{\text{g}} \to \text{b}\bar{\text{b}}\tilde{\chi}_1^0$ $m_{\tilde{\text{g}}} = 1500$ GeV $m_{\tilde{\chi}_1^0} = 100$ GeV	$pp \to \tilde{\text{g}}\tilde{\text{g}}, \tilde{\text{g}} \to \text{t}\bar{\text{t}}\tilde{\chi}_1^0$ $m_{\tilde{\text{g}}} = 1500$ GeV $m_{\tilde{\chi}_1^0} = 100$ GeV	$pp \to \tilde{\text{g}}\tilde{\text{g}}, \tilde{\text{g}} \to \text{q}\bar{\text{q}}\tilde{\chi}_1^0$ $m_{\tilde{\text{g}}} = 1000$ GeV $m_{\tilde{\chi}_1^0} = 800$ GeV
1	200-500	500-800	0	0.01 ± 0.00	0.00 ± 0.00	58.45 ± 1.09
2	200-500	800-1200	0	0.05 ± 0.00	0.00 ± 0.00	13.30 ± 0.51
3	200-500	1200+	0	0.63 ± 0.02	0.03 ± 0.00	1.36 ± 0.16
4	500-750	500-1200	0	0.05 ± 0.00	0.01 ± 0.00	10.80 ± 0.50
5	500-750	1200+	0	0.55 ± 0.01	0.03 ± 0.00	2.13 ± 0.21
6	750+	800+	0	0.58 ± 0.01	0.03 ± 0.00	3.48 ± 0.27
7	200-500	500-800	1	0.03 ± 0.00	0.01 ± 0.00	11.60 ± 0.27
8	200-500	800-1200	1	0.19 ± 0.01	0.01 ± 0.00	3.15 ± 0.14
9	200-500	1200+	1	1.73 ± 0.04	0.06 ± 0.00	0.27 ± 0.04
10	500-750	500-1200	1	0.20 ± 0.01	0.02 ± 0.00	2.25 ± 0.12
11	500-750	1200+	1	1.58 ± 0.03	0.06 ± 0.01	0.43 ± 0.05
12	750+	800+	1	1.73 ± 0.03	0.07 ± 0.01	0.58 ± 0.06
13	200-500	500-800	2	0.04 ± 0.01	0.01 ± 0.00	1.26 ± 0.05
14	200-500	800-1200	2	0.29 ± 0.01	0.01 ± 0.00	0.38 ± 0.03
15	200-500	1200+	2	1.79 ± 0.04	0.05 ± 0.00	0.03 ± 0.01
16	500-750	500-1200	2	0.29 ± 0.02	0.02 ± 0.00	0.27 ± 0.03
17	500-750	1200+	2	1.72 ± 0.03	0.05 ± 0.00	0.04 ± 0.01
18	750+	800+	2	1.89 ± 0.04	0.06 ± 0.00	0.05 ± 0.01
19	200-500	500-800	3+	0.03 ± 0.01	0.00 ± 0.00	0.08 ± 0.01
20	200-500	800-1200	3+	0.25 ± 0.01	0.01 ± 0.00	0.04 ± 0.01
21	200-500	1200+	3+	1.06 ± 0.03	0.02 ± 0.00	0.00 ± 0.00
22	500-750	500-1200	3+	0.25 ± 0.02	0.01 ± 0.00	0.02 ± 0.00
23	500-750	1200+	3+	1.04 ± 0.03	0.03 ± 0.00	0.00 ± 0.00
24	750+	800+	3+	1.10 ± 0.03	0.03 ± 0.00	0.00 ± 0.00

Table 2: Expected numbers of events in search bins with $7 \leq N_{\text{jet}} \leq 8$ for three representative signal models. Only statistical uncertainties are shown.

Bin	$H_{\text{T}}^{\text{miss}}$ [GeV]	H_{T} [GeV]	$N_{\text{b-jet}}$	$pp \to \tilde{\text{g}}\tilde{\text{g}}, \tilde{\text{g}} \to \text{b}\bar{\text{b}}\tilde{\chi}_1^0$ $m_{\tilde{\text{g}}} = 1500$ GeV $m_{\tilde{\chi}_1^0} = 100$ GeV	$pp \to \tilde{\text{g}}\tilde{\text{g}}, \tilde{\text{g}} \to \text{t}\bar{\text{t}}\tilde{\chi}_1^0$ $m_{\tilde{\text{g}}} = 1500$ GeV $m_{\tilde{\chi}_1^0} = 100$ GeV	$pp \to \tilde{\text{g}}\tilde{\text{g}}, \tilde{\text{g}} \to \text{q}\bar{\text{q}}\tilde{\chi}_1^0$ $m_{\tilde{\text{g}}} = 1000$ GeV $m_{\tilde{\chi}_1^0} = 800$ GeV
25	200-500	500-800	0	0.00 ± 0.00	0.00 ± 0.00	14.25 ± 0.52
26	200-500	800-1200	0	0.01 ± 0.00	0.01 ± 0.00	10.67 ± 0.46
27	200-500	1200+	0	0.20 ± 0.01	0.08 ± 0.00	2.37 ± 0.21
28	500-750	500-1200	0	0.00 ± 0.00	0.01 ± 0.00	3.68 ± 0.27
29	500-750	1200+	0	0.17 ± 0.01	0.07 ± 0.00	1.86 ± 0.19
30	750+	800+	0	0.17 ± 0.01	0.06 ± 0.00	1.92 ± 0.19
31	200-500	500-800	1	0.00 ± 0.00	0.01 ± 0.00	3.80 ± 0.17
32	200-500	800-1200	1	0.03 ± 0.00	0.04 ± 0.00	2.96 ± 0.15
33	200-500	1200+	1	0.65 ± 0.02	0.26 ± 0.01	0.70 ± 0.07
34	500-750	500-1200	1	0.02 ± 0.00	0.04 ± 0.00	1.13 ± 0.09
35	500-750	1200+	1	0.58 ± 0.02	0.21 ± 0.01	0.57 ± 0.06
36	750+	800+	1	0.58 ± 0.02	0.22 ± 0.01	0.45 ± 0.05
37	200-500	500-800	2	0.00 ± 0.00	0.01 ± 0.00	0.62 ± 0.05
38	200-500	800-1200	2	0.05 ± 0.01	0.06 ± 0.00	0.49 ± 0.04
39	200-500	1200+	2	0.81 ± 0.02	0.32 ± 0.01	0.16 ± 0.03
40	500-750	500-1200	2	0.04 ± 0.00	0.06 ± 0.00	0.19 ± 0.03
41	500-750	1200+	2	0.74 ± 0.02	0.26 ± 0.01	0.11 ± 0.02
42	750+	800+	2	0.74 ± 0.02	0.28 ± 0.01	0.07 ± 0.01
43	200-500	500-800	3+	0.00 ± 0.00	0.01 ± 0.00	0.08 ± 0.02
44	200-500	800-1200	3+	0.06 ± 0.01	0.06 ± 0.00	0.05 ± 0.01
45	200-500	1200+	3+	0.65 ± 0.02	0.26 ± 0.01	0.03 ± 0.01
46	500-750	500-1200	3+	0.04 ± 0.01	0.06 ± 0.00	0.02 ± 0.00
47	500-750	1200+	3+	0.59 ± 0.02	0.20 ± 0.01	0.02 ± 0.01
48	750+	800+	3+	0.57 ± 0.02	0.22 ± 0.01	0.01 ± 0.00

Table 3: Expected numbers of events in search bins with $N_{\text{jet}} \geq 9$ for three representative signal models. Only statistical uncertainties are shown.

Bin	$H_{\text{T}}^{\text{miss}}$ [GeV]	H_{T} [GeV]	$N_{\text{b-jet}}$	$pp \to \tilde{\text{g}}\tilde{\text{g}}, \tilde{\text{g}} \to \text{b}\bar{\text{b}}\tilde{\chi}_1^0$ $m_{\tilde{\text{g}}} = 1500$ GeV $m_{\tilde{\chi}_1^0} = 100$ GeV	$pp \to \tilde{\text{g}}\tilde{\text{g}}, \tilde{\text{g}} \to \text{t}\bar{\text{t}}\tilde{\chi}_1^0$ $m_{\tilde{\text{g}}} = 1500$ GeV $m_{\tilde{\chi}_1^0} = 100$ GeV	$pp \to \tilde{\text{g}}\tilde{\text{g}}, \tilde{\text{g}} \to \text{q}\bar{\text{q}}\tilde{\chi}_1^0$ $m_{\tilde{\text{g}}} = 1000$ GeV $m_{\tilde{\chi}_1^0} = 800$ GeV
49	200-500	500-800	0	0.00 ± 0.00	0.00 ± 0.00	1.16 ± 0.14
50	200-500	800-1200	0	0.00 ± 0.00	0.01 ± 0.00	2.64 ± 0.22
51	200-500	1200+	0	0.06 ± 0.00	0.12 ± 0.00	1.06 ± 0.13
52	500-750	500-1200	0	0.00 ± 0.00	0.01 ± 0.00	0.64 ± 0.11
53	500-750	1200+	0	0.05 ± 0.00	0.10 ± 0.00	0.88 ± 0.12
54	750+	800+	0	0.04 ± 0.00	0.08 ± 0.00	0.85 ± 0.12
55	200-500	500-800	1	0.00 ± 0.00	0.00 ± 0.00	0.38 ± 0.05
56	200-500	800-1200	1	0.00 ± 0.00	0.04 ± 0.00	1.08 ± 0.10
57	200-500	1200+	1	0.20 ± 0.01	0.49 ± 0.01	0.44 ± 0.06
58	500-750	500-1200	1	0.00 ± 0.00	0.03 ± 0.00	0.22 ± 0.04
59	500-750	1200+	1	0.18 ± 0.01	0.42 ± 0.01	0.36 ± 0.05
60	750+	800+	1	0.15 ± 0.01	0.34 ± 0.01	0.37 ± 0.06
61	200-500	500-800	2	0.00 ± 0.00	0.00 ± 0.00	0.07 ± 0.01
62	200-500	800-1200	2	0.01 ± 0.00	0.07 ± 0.00	0.26 ± 0.04
63	200-500	1200+	2	0.29 ± 0.01	0.81 ± 0.02	0.12 ± 0.03
64	500-750	500-1200	2	0.00 ± 0.00	0.05 ± 0.00	0.04 ± 0.01
65	500-750	1200+	2	0.25 ± 0.01	0.71 ± 0.02	0.10 ± 0.02
66	750+	800+	2	0.21 ± 0.01	0.54 ± 0.01	0.12 ± 0.03
67	200-500	500-800	3+	0.00 ± 0.00	0.01 ± 0.00	0.01 ± 0.00
68	200-500	800-1200	3+	0.01 ± 0.00	0.08 ± 0.01	0.05 ± 0.01
69	200-500	1200+	3+	0.29 ± 0.02	1.02 ± 0.02	0.02 ± 0.01
70	500-750	500-1200	3+	0.00 ± 0.00	0.06 ± 0.00	0.00 ± 0.00
71	500-750	1200+	3+	0.26 ± 0.01	0.89 ± 0.02	0.02 ± 0.01
72	750+	800+	3+	0.21 ± 0.01	0.65 ± 0.02	0.02 ± 0.01